JOURNAL OF COMPUTATIONAL PHYSICS **139,** 79–91 (1998)
ARTICLE NO. CP975864

Linear Stability Analysis of Thermo-Lattice Boltzmann Models

Pavol Pavlo,* George Vahala,†,‡ Linda Vahala,§ and Min Soe†

*Institute of Plasma Physics, Academic Science, Czech Republic; †Department of Physics, William & Mary, Williamsburg, Virginia 23187; ‡ICASE, NASA-Langley, Hampton, Virginia 23681; §Department of Electrical & Computer Engineering, Old Dominion University, Norfolk, Virginia 23529; †Department of Physics, William & Mary, Williamsburg, Virginia 23187

Received March 31, 1997; revised October 6, 1997

The numerical stability of thermo-lattice Boltzmann (TLBE) models is presented. The TLBE algorithm is linearized and represented in matrix form. The spectral radius of the resulting matrix is obtained by the method of powers. In particular, the numerical stability of two 2-speed 13-bit TLBE models—one based on the hexagonal lattice, and the other on a square lattice—is examined. For these two TLBE models, as a function of the energy density, the achievable Reynolds number (before the onset of grid modes) is more than an order of magnitude greater for the hexagonal grid than for the square grid. © 1998 Academic Press

1. INTRODUCTION

With the advent of massively parallel platforms, lattice gas (LGA) and lattice Boltzmann (LBE) methods [1–4] have surfaced as interesting contenders for the computational fluid dynamic simulations of complex flows. In attempts to overcome the early well-known defects of LGA (e.g., lack of Galilean invariance in the fluid equations, pressure as a function of the mean velocity), LBE methods were constructed in which the collision matrix was simplified to a simple BGK [5] collisional relaxation and the Boolean algebra was replaced by distribution functions. However, in drifting away from the LGA Boolean detailed collisional microdynamics with its H-theorems and absolute stability [6], LBE is left without these moorings. Alternatively, LBE methods can be viewed in their own right as an explicit finite-difference Lagrangian technique [7] to solve nonlinear macroscopic problems.

LBE methods to simulate nearly incompressible Navier–Stokes have been successful, with detailed benchmarking for some two-dimensional (2D) flows [8]. The linearized Boltzmann equation with single-time BGK collisional relaxation term is solved on a discrete spatial lattice so chosen [2] that the discrete microscopic lattice symmetries do not taint the long wavelength, large time Chapman–Enskog limit of rotationally symmetric macroscopic

0021-9991/98 $25.00

dynamics. For 2D flows, the 9-bit square grid and the 7-bit hexagonal grid have the required symmetry and in the Chapman–Enskog limit are closed at the mass and momentum conservation levels. Besides the near incompressibility issue, these early LBE models recovered the quadratically nonlinear Navier–Stokes momentum equation—but they also introduced spurious cubic nonlinearities [9] because of the truncation level of the Taylor expansion for the chosen relaxed distribution function in the BGK collision operator. These cubic nonlinearities can be eliminated [10] from the momentum equation by going to higher order in the Taylor expansion and working with the 9-bit square grid.

Forays have also been made into thermo-lattice Boltzmann (TLBE) models [11–13] for compressible flows with macroscopic closure at the mass, momentum, and energy conservation levels. At the simplest level for 2D flows, this requires a 13-bit model for either the square [13] or hexagonal [11] grid. Moreover, we [14, 15] have found the hexagonal lattice model of Alexander *et al.* [11] to be practically usable and computationally very efficient within certain parameter windows while the square lattice models are plagued by grid mode instabilities [7]. Now it has been claimed [10] that the spurious macroscopic nonquadratic nonlinearities in the momentum and energy equations can only be successfully removed on a square lattice, but not on a hexagonal grid.

Faced with this dichotomy, it is thus important to consider the numerical stability of both the hexagonal and square TLBE models—but to date very little attention has been paid to this issue in TLBE. However, there has been some discussion of linear stability of the square and hexagonal grids in LBE. Benzi *et al.* [16] have discussed linear stability for equilibrium distribution functions with zero mean velocity, while Stirling and Chen [17] have examined LBE linear stability with nonzero mean velocity. These need not be equivalent since one only requires LBE to enforce Galilean invariance at the fluid level. With linearization of the equilibrium distribution functions about zero mean velocity in LBE, instabilities are wavenumber independent and are only dependent on the eigenvalues of the linearized collision operator [16]. On the other hand, the dynamics of the fluctuations about nonzero mean velocities the equilibria are much more prone to instabilities because of the effect of mode–mode coupling [16] between the various speeds needed in the LBE model. This mode–mode coupling can give rise to short-wavelength modes that drive the distribution functions negative at some lattice nodes and numerical instability. These instabilities were examined in detail by Stirling and Chen [17]. Here we look at TLBE which includes closure at the energy level. Hence we shall examine linear stability about zero mean velocity (since all LBE and TLBE studies involve only small mean velocities) but finite energy (of course, in LBE, energy never enters into the fluid equations). Thus, we will also be faced with mode–mode induced short-wavelength instabilities, now driven by the nonzero energy. However, unlike Stirling and Chen [17], who perform a von Neumann linear stability analysis on LBE for particular wavenumbers, we perform a global quantitative linear stability of TLBE. From this analysis, we determine optimal parameter regimes and estimate the achievable Reynolds number. For 2D flows, we compare the numerical stability of the hexagonal and square lattice TLBE models. It should be pointed out that our method can be readily applied to 3D flows.

2. MACROSCOPIC LINEARIZATION OF TLBE

One first defines a set of base vectors to represent the allowed discrete velocities in the TLBE model

$$\{\mathbf{e}_{pi}\}, \quad i = 1\ldots, b_p;\ p = 1.\ldots n_p. \tag{1}$$

The index i runs over those base vectors of speed $e_p = |\mathbf{e}_{pi}|$, while the index p runs over all the allowed speeds. If rest particles are included, then p = 0 with $\mathbf{e}_0 = \mathbf{0}$, and $b_0 = 1$. Thus for the 2-speed 13-bit hexagonal TLBE model of Alexander *et al.* [11], we have $b_p = 6$, $n_p = 2$, as well as the rest particle. The total number of bits in a model is just

$$n_s = \sum_{p=0}^{n_p} b_p. \tag{2}$$

The base vectors are so chosen that for all (but the boundary) spatial lattice nodes $\mathbf{x_k}$, the vector $\mathbf{x_p} + \mathbf{e}_{pi}$ is also a spatial lattice node for all p and i.

Further, the particle distribution function is discretized in both space and velocity so that $N_{pi}(\mathbf{x_k})$ is the number of particles at the node $\mathbf{x_k}$ moving with the velocity $\mathbf{e}_{pi}$. In TLBE, the dynamics of the system is governed by the linearized Boltzmann equation with single relaxation collision operator

$$N_{pi}(\mathbf{x_k} + \mathbf{e}_{pi}, t + 1) - N_{pi}(\mathbf{x_k}, t) = -\frac{1}{\tau}\left[N_{pi}(\mathbf{x_k}, t) - N^{eq}_{pi}(\mathbf{x_k}, t)\right], \tag{3}$$

where τ is the relaxation time which governs how rapidly the distribution function $N_{pi}(\mathbf{x_k})$ is driven towards the equilibrium distribution function $N^{eq}_{pi}(\mathbf{x_k})$. In standard lattice Boltzmann methods, the equilibrium distribution function $N^{eq}_{pi}(\mathbf{x_k})$ is assumed to be a truncated Taylor series in the mean flow $\mathbf{u}$ with the coefficients satisfying certain isotropic constraints and collisional invariants. In particular, one needs to force the BGK collision operator (the r.h.s. of (3)) to conserve particle density ρ, momentum $\rho\mathbf{u}$, and energy density ε:

$$\sum_{pi} N^{eq}_{pi} = \rho, \quad \sum_{pi} N^{eq}_{pi}\mathbf{e}_{pi} = \rho\mathbf{u}, \quad \sum_{pi} N^{eq}_{pi} e_p^2 = 2\rho\varepsilon + \rho u^2. \tag{4}$$

A typical TLBE equilibrium distribution function [11–13] has the form

$$N^{eq}_{pi} = \rho[A_p(\varepsilon) + B_p(\varepsilon)\mathbf{e}_{pi} \cdot \mathbf{u} + O(u^2, \varepsilon u..)], \tag{5}$$

where the coefficients

$$A_p(\varepsilon) = a_{p0} + a_{p1}\varepsilon + a_{p2}\varepsilon^2, \quad B_p(\varepsilon) = b_{p0} + b_{p1}\varepsilon, \tag{6}$$

and the particular a_{p0} are dependent on the specific lattice chosen.

The LBE algorithm, (3), requires a very simple two-step process: (a) the free-streaming of the distribution functions N_{pi} from node $\mathbf{x_k}$ to the node $\mathbf{x_k} + \mathbf{e}_{pi}$ which is just a shift operation; and (b) BGK collisional relaxation at each node site. Thus all operations are purely local and are wonderfully suited for parallelization on multinode computers.

We now proceed to the (macroscopic) linearization of TLBE in preparation for the stability analysis. Since typical mean velocities in both LBE and TLBE simulations are small, it is appropriate to consider the unperturbed macrostate (at t = 0) at each node:

$$\rho(\mathbf{x_k}) = \rho_0 = 1; \quad \mathbf{u}(\mathbf{x_k}) = 0; \quad \varepsilon(\mathbf{x_k}) = \varepsilon_0, \tag{7}$$

so that the equilibrium distribution function

$$N^{eq}_{pi}(\varepsilon = \varepsilon_0, \mathbf{u} = 0) = A^0_p, \tag{8}$$

where

$$\mathrm{A}_{\mathrm{p}}^{0} \equiv \mathrm{A}_{\mathrm{p}}(\varepsilon_0), \quad \text{for all } \mathbf{x}_{\mathbf{k}}. \tag{9}$$

Now apply an arbitrary perturbation $\xi_{\pi i}^{(0)}(\mathbf{x}_{\mathbf{k}})$ to this equilibrium, so that

(I) at time t = 0 (notation$^{(0)}$):

$$\mathrm{N}_{\mathrm{pi}}^{(0)}(\mathbf{x}_{\mathbf{k}}) = \mathrm{A}_{\mathrm{p}}^{0} + \xi_{\mathrm{pi}}^{(0)}(\mathbf{x}_{\mathbf{k}}) \tag{10}$$

and

(II) at time t = 1 (notation$^{(1,\mathrm{s})}$) after the free-streaming, but before the collisional relaxation step,

$$\mathrm{N}_{\mathrm{pi}}^{(1,\mathrm{s})}(\mathbf{x}_{\mathbf{k}}) = \mathrm{A}_{\mathrm{p}}^{0} + \xi_{\mathrm{pi}}^{(0)}(\mathbf{x}_{\mathbf{k}} - \mathbf{e}_{\mathrm{pi}}). \tag{11}$$

To determine the equilibrium distribution at the next time step, (5), we need to calculate the new macroscopic variables $\rho^{(1)}$, $\rho^{(1)}\mathbf{u}^{(1)}$, $\rho^{(1)}\varepsilon^{(1)}$,

$$\begin{aligned}
\rho^{(1)}(\mathbf{x}_{\mathbf{k}}) &= \sum_{\mathrm{pi}} \mathrm{N}_{\mathrm{pi}}^{(1,\mathrm{s})}(\mathbf{x}_{\mathbf{k}}) = 1 + \sum_{\mathrm{pi}} \xi_{\mathrm{pi}}^{(0)}(\mathbf{x}_{\mathbf{k}} - \mathbf{e}_{\mathrm{pi}}) \\
\rho^{(1)}(\mathbf{x}_{\mathbf{k}})\mathbf{u}^{(1)}(\mathbf{x}_{\mathbf{k}}) &= \sum_{\mathrm{pi}} \boldsymbol{e}_{\mathrm{pi}} \mathrm{N}_{\mathrm{pi}}^{(1,\mathrm{s})}(\mathbf{x}_{\mathbf{k}}) = \sum_{\mathrm{pi}} \boldsymbol{e}_{\mathrm{pi}}\, \xi_{\mathrm{pi}}^{(0)}(\mathbf{x}_{\mathbf{k}} - \mathbf{e}_{\mathrm{pi}}) \\
2\rho^{(1)}(\mathbf{x}_{\mathbf{k}})\varepsilon^{(1)}(\mathbf{x}_{\mathbf{k}}) &= \sum_{\mathrm{pi}} \mathrm{e}_{\mathrm{p}}^{2}\, \mathrm{N}_{\mathrm{pi}}^{(1,\mathrm{s})}(\mathbf{x}_{\mathbf{k}}) - \rho^{(1)}(\mathbf{x}_{\mathbf{k}})\mathrm{u}^{2}(\mathbf{x}_{\mathrm{k}}) \\
&= 2\varepsilon_0 - \rho^{(1)}(\mathbf{x}_{\mathbf{k}})[\mathrm{u}^{(1)}(\mathbf{x}_{\mathbf{k}})]^2 + \sum_{\mathrm{pi}} \mathrm{e}_{\mathrm{p}}^{2}\, \xi_{\mathrm{pi}}^{(0)}(\mathbf{x}_{\mathbf{k}} - \mathbf{e}_{\mathrm{pi}})
\end{aligned} \tag{12}$$

on using (4)–(11). On Taylor-expanding the equilibrium distribution function around the unperturbed macrostate (7),

$$\begin{aligned}
\mathrm{N}_{\mathrm{pi}}^{(1,\mathrm{eq})} &= \rho^{(1)}\left[\mathrm{A}_{\mathrm{p}}^{0} + (\varepsilon - \varepsilon_0)\mathrm{A}_{\mathrm{p}}^{\prime 0} + (\mathbf{e}_{\mathrm{pi}} \cdot \mathbf{u})\mathrm{B}_{\mathrm{p}}^{0} + \cdots\right] \\
&= \mathrm{A}_{\mathrm{p}}^{\prime 0} + \sum_{\mathrm{qj}} \left\{ \mathrm{A}_{\mathrm{p}}^{0} + \left(\frac{\mathrm{e}_{\mathrm{q}}^{2}}{2} - \varepsilon_0 \right) \mathrm{A}_{\mathrm{p}}^{\prime 0} + (\mathbf{e}_{\mathrm{pi}} \cdot \mathbf{e}_{\mathrm{qj}})\, \mathrm{B}_{\mathrm{p}}^{0} \right\} \xi_{\mathrm{qj}}^{(0)}(\mathbf{x}_{\mathbf{k}} - \mathbf{e}_{\mathrm{qj}}) + \cdots,
\end{aligned} \tag{13}$$

on neglecting terms of $\mathrm{O}(\xi^2)$. Here the derivative $\mathrm{A}_{\mathrm{p}}^{\prime 0} \equiv \mathrm{A}'(\varepsilon_0)$ and $\mathrm{B}_{\mathrm{p}}^{0} \equiv \mathrm{B}_{\mathrm{p}}(\varepsilon_0)$.

(III) At time t = 1, after the collision relaxation: the distributions $\mathrm{N}_{\mathrm{pi}}^{(1)}(\mathbf{x}_{\mathbf{k}})$ can be determined from the equilibrium distribution (13) and the TLBE evolution equation (3). The perturbed distribution at time t = 1,

$$\begin{aligned}
\xi_{\mathrm{pi}}^{(1)}(\mathbf{x}_{\mathbf{k}}) &= \mathrm{N}_{\mathrm{pi}}^{(1)}(\mathbf{x}_{\mathbf{k}}) - \mathrm{A}_{\mathrm{p}}^{0} \\
&= \sum_{\mathrm{qj}} \left[\frac{1}{\tau} \left\{ \mathrm{A}_{\mathrm{p}}^{0} + \left(\frac{\mathrm{e}_{\mathrm{q}}^{2}}{2} - \varepsilon_0 \right) \mathrm{A}_{\mathrm{p}}^{\prime 0} + (\mathbf{e}_{\mathrm{pi}} \cdot \mathbf{e}_{\mathrm{q}}) \mathrm{B}_{\mathrm{p}}^{0} \right\} \right. \\
&\qquad \left. + \left(1 - \frac{1}{\tau} \right) \delta_{\mathrm{pq}} \delta_{\mathrm{ij}} \right] \xi_{\mathrm{qj}}^{(0)}(\mathbf{x}_{\mathbf{k}} - \mathbf{e}_{\mathrm{qj}}),
\end{aligned} \tag{14}$$

where δ_{ij} is the standard Kronecker symbol.

It is convenient to relabel the lattice nodes by a single index k : k = 1, ... , J, where

$$J = \prod_{\alpha=1}^{D} n_\alpha. \tag{15}$$

Here n_α is the number of nodes in the αth direction in D dimension space. We also rewrite the set of all perturbation distribution functions $\{\xi_{pi}(\mathbf{x_k})\}$ into a vector Ξ of length $J \times n_s$, where n_s is the total number of bits in the simulation, (2). Finally, we introduce an isomorphic map M of indices (p, i, k) into the single index m,

$$m = M(p, i, k) \tag{16}$$

so that at time t

$$\Xi_m^{(t)} \equiv \xi_{pi}^{(t)}(\mathbf{x_k}), \quad m = 1 \cdots M, \text{ where } M \equiv Jn_s. \tag{17}$$

With this indexing, we define an M × M matrix C with elements

$$c_{mn} = \left[\frac{1}{\tau}\left\{A_p^0 + \left(\frac{e_q^2}{2} - \varepsilon_0\right)A_p'^0 + (\mathbf{e}_{pi} \cdot \mathbf{e}_{qj})B_p^0\right\} + \left\{1 - \frac{1}{\tau}\right\}\delta_{pq}\delta_{ij}\right]\delta_{\mathbf{kl}} \tag{18}$$

and an M × M matrix **S** with delta-function elements

$$s_{mn} = \delta_{pq}\delta_{ij}\delta(\mathbf{x_l} - \mathbf{x_k} - \mathbf{e}_{qj}). \tag{19}$$

Here

$$n = M(q, j, 1). \tag{20}$$

Thus the study of the linear stability of TLBE has been reduced to an eigenvalue problem of the form

$$\Xi^{(t+1)} = \mathbf{CS}\Xi^{(t)}. \tag{21}$$

The **C** matrix is related to the collisional relaxation operation (with the δ_{kl} in (18) reflecting its local character) and is block-diagonal. The **S** matrix represents the streaming operation; it shifts ξ_{pi} from node $\mathbf{x_k} - \mathbf{e}_{pi}$ to the node $\mathbf{x_k}$.

3. LINEAR STABILITY ANALYSIS

The first thing to note is the dimensionality of the matrix **C** · **S**: for a 2D 13-bit TLBE model on a 512 × 512 grid, the dimensionality is on the order of 3.4e+06 × 3.4e+06. The matrix **C** · **S** is real but asymmetric, even for just one moving speed ($n_p \geq 1$) if the rest particles are included, as is required for TLBE under any chosen lattice.

Without appealing to the tremendous memory requirements for a matrix of this size, it is impossible to use the standard tools of eigenvalue analysis because of the accumulation of numerical errors. In practice, the maximal (physical) size of a lattice system that is tractable by standard procedures (e.g., as contained in the NAG library or IDL) turned out to be only

a 4×4 grid for the 2-speed 13-bit TLBE model. However, we have found that the results obtained on such small lattice systems prove to be irrelevant (see Section 4).

However, the form of the matrix $\mathbf{C} \cdot \mathbf{S}$ allows for efficient algorithms in applying iterative methods. First, we note that the matrix $\mathbf{C}$ is composed of J identical $n_s \times n_s$ blocks. The rest of the elements are zero, so only one block needs to be kept in memory. Moreover, instead of using the full streaming matrix $\mathbf{S}$ we can apply, between successive iterations, the streaming rules to move the elements of the perturbation vector Ξ to their new positions. In other words, we can fully utilize the LBE algorithm, with the collision operator (14) replacing (3); the definitions (18)–(19) are given here for convenience.

From the stability point of view, we are only interested in the spectral radius ρ_λ of the matrix $\mathbf{C} \cdot \mathbf{S}$, i.e. in the maximum absolute value of all its eigenvalues $\{\lambda_m\}$. For this purpose we adopt the method of powers [18]. Suppose that the $M \times M$ matrix $\mathbf{A}$ has M linearly independent eigenvectors $\mathbf{w}_m$ with corresponding eigenvalues λ_m, $m = 1 \cdots M$. An arbitrary vector $\mathbf{v}_0$ can then be expressed as

$$\mathbf{v}_0 = \sum_{m=1}^{M} \alpha_m \mathbf{w}_m \tag{22}$$

so that the nth iterated vector $\mathbf{v}_n$

$$\mathbf{v}_n = \mathbf{A}^n \mathbf{v}_0 = \sum_{m=1}^{M} \lambda_m^n \alpha_m \mathbf{w}_m. \tag{23}$$

Let λ_1 be the dominant eigenvalue: $|\lambda_1| > |\lambda_m|$ for all $m > 1$. Provided $\mathbf{v}_0$ is not orthogonal to $\mathbf{w}_1$ (so that $\alpha_1 \neq 0$), it is known that

$$\lim_{n\to\infty} \frac{1}{\lambda_1^n} \mathbf{A}^n \mathbf{v}_0 = \alpha_1 \mathbf{w}_1 \tag{24}$$

so that

$$\lambda_1 = \lim_{n\to\infty} \frac{(\mathbf{y} \cdot \mathbf{v}_{n+1})}{(\mathbf{y} \cdot \mathbf{v}_n)} \tag{25}$$

for any vector $\mathbf{y}$ not orthogonal to $\mathbf{w}_1$. In practice, for the nth approximation of the leading eigenvalue $\lambda_1^{(n)}$, one takes the quotient of the maximum components of two successive vectors $\mathbf{v}_n$ and $\mathbf{v}_{n+1}$.

The convergence to λ_1 in (25) is guaranteed only if a dominant (single or multiple) real eigenvalue exists. It is easy to derive a similar expression for the case in which a single complex pair of eigenvalues dominates. Strictly speaking, one would have to treat individually all special cases (i.e., all possible combinations of real and complex eigenvalues of the same (maximum) absolute values). However, this is just impossible considering the number of eigenvalues involved. Instead of this, if (25) fails to converge, we take a long-time geometric average

$$\left|\lambda_i^{(n)}\right| = \left[\frac{F_{max}^{(n)}}{F_{max}^{(n-I)}}\right]^{1/I}, \tag{26}$$

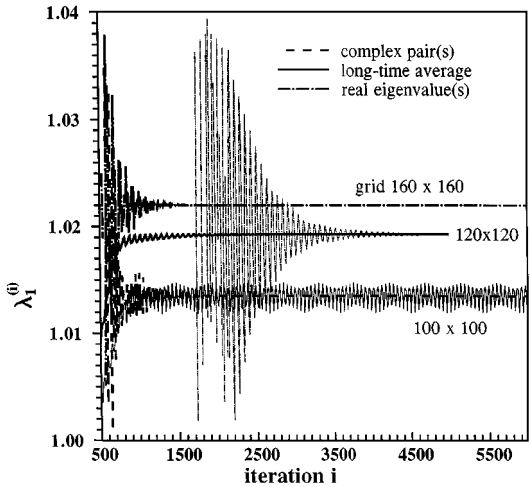

FIG. 1. For energy density $\varepsilon_0 = 0.3$, the evolution of the dominant eigenvalue $\lambda_1^{(i)}$ as a function of the iteration i for three different hexagonal lattices: 100×100, 120×120, and 160×160. The dominant eigenvalue structure changes with the size of the lattice. The dashed-dot curve is calculated from Eq. (25), the full line from the long-time average Eq. (26). For $i < 1500$, the amplitude of the oscillations for the 120×120 lattice are off-scale.

where

$$F_{max}^{(n)} \equiv \max \left\{ \xi_{pi}^{(n)}(\mathbf{x_k}) \right\} \tag{27}$$

with suitably chosen span **I**. In what follows, this value $|\lambda_1|$ will be referred to as the spectral radius ρ_λ.

A few cases are illustrated in Fig. 1. As a rule, (25) yields satisfactory convergence (dash-dotted lines), although the long-time average (26) may converge faster (full lines, $\mathbf{I} = 400$). Rarely, even (26) may fail. This occurs when dominant eigenvalues are complex and have modulus very close to unity (dashed line). Hence, the method of powers must be used with some supervision—although we did not encounter any of these difficulties when a sufficiently large number of lattice nodes were employed in the TLBE simulation.

The relevance of the linear stability analysis to the full TLBE system is considered in Fig. 2. The full line is the spectral radius as calculated by the above procedures for the hexagonal grid [11], as described in the next section. For comparison, we have run a full TLBE double shear code [15] based on the same model with $\tau = 0.5$. N_f in the Fig. 2 is the timestep when, due to excitation of eigenmodes, some of the distributions $N_{pi}(\mathbf{x_k})$ become negative (dashed-dotted line). Note that the eigenmodes grow exponentially with time, $e^{\gamma \cdot t}$, with the most unstable eigenmode having its growth rate $\gamma \propto N_f^{-1}$. In one timestep, the mode amplitude has increased by e^{γ}. In the linear stability study, the spectral radius $\rho_\lambda = |\lambda_1|$ so that

$$\rho_\lambda \approx \exp\left[\text{const} \times N_f^{-1} \right]. \tag{28}$$

This is verified in the Fig. 2 (cf., the squares).

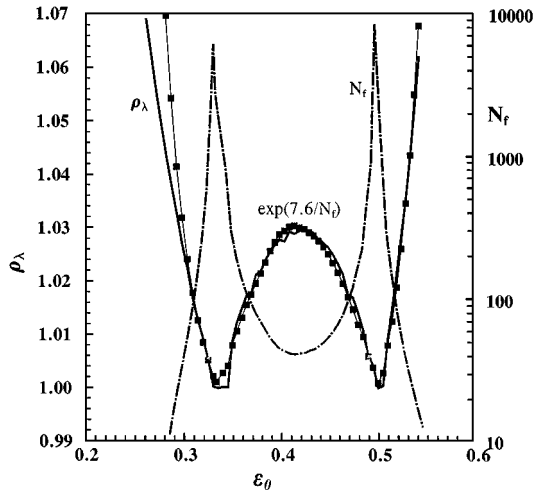

FIG. 2. A plot of the spectral radius ρ_λ as a function of the energy density ε_0 at $\tau = 0.5$, as well as a plot of the time iteration number N_f, at which one of the distribution functions becomes negative for the hexagonal TLBE model [11]. $\tau = 0.5$ corresponds to infinite Reynolds $R_H = \infty(\nu = 0)$, and numerical instability $\rho_\lambda > 1$. However, there are two regions in energy density ε_0, where locally some of the distribution functions become negative after 4000 time steps (N_f): one window is around $\varepsilon_0 \approx 0.33$; a narrower window is around $\varepsilon_0 \approx 0.5$. Within these windows the spectral radius $\rho_\lambda = 1+$. The curve with the squares is a curve fit of the spectral radius as a function of N_f for each energy density ε_0.

4. LINEAR STABILITY OF TLBE MODELS ON HEXAGONAL AND SQUARE GRID

In this section, we compare the linear stability between two 2D 13-bit TLBE models:

(I) the 2-speed hexagonal lattice model of Alexander *et al.* [11] with the base vector components

$$\mathbf{e}_0 = \mathbf{0}, \quad \mathbf{e}_{pi} = e_p(\cos\beta_i, \sin\beta_i) \quad \text{with } e_p = p = 1, 2 \text{ and } \beta_i = \frac{(i-1)\pi}{3}, \quad i = 1 \cdots \epsilon, \tag{29}$$

(II) the 3-speed square model of Qian [13] with base vector components

$$\begin{aligned} &\mathbf{e}_0 = \mathbf{0}, \quad \mathbf{e}_{pi} = e_p(\cos\beta_i, \sin\beta_i) \quad \text{with } p = 1, 3; \\ &e_1 = 1, e_3 = 2, \text{ and } \beta_i = \frac{(i-1)\pi}{2}, \quad i = 1 \cdots 4, \\ &\mathbf{e}_{pi} = e_p(\cos\beta_i, \sin\beta_i) \quad \text{with } p = 2; e_2 = 2^{1/2}, \text{ and} \\ &\beta_i = \frac{(i-1/2)\pi}{2}, \quad i = 1 \cdots 4; \end{aligned} \tag{30}$$

i.e., in the Qian model there are eight bits along the Cartesian axes and four bits along the diagonals.

Note that these two models are accurate to the same level (fourth-rank tensor isotropy with the tensor composed from the base vectors) and are computationally equivalent (both

13 bits). The only adjustable parameter in both these models is the initial internal energy density ε_0. The kinematic viscosity ν [11, 13] is related to the relaxation rate τ

$$\nu = \frac{3}{2}\varepsilon\left(\tau - \frac{1}{2}\right) \tag{31}$$

so that the corresponding Reynolds number

$$\mathrm{R} = \frac{4\mathrm{u}}{3\varepsilon}\,\frac{\mathrm{n}_\alpha}{(2\tau - 1)}. \tag{32}$$

Equations (31) and (32) are independent of the lattice geometry, and we shall denote by $\mathrm{R_H}$ and $\mathrm{R_R}$ the Reynolds number for the hexagonal and square grids, respectively.

We first consider the dependence of the spectral radius ρ_λ on the number of lattice nodes J, (15), at zero viscosity $\nu = 0$, (31). In Fig. 3 we plot ρ_λ as a function of ε_0 for relaxation parameter $\tau = 0.5$, a parameter value that must be unstable since it corresponds to infinite Reynolds number, (32). The spectral radius for the hexagonal grid is shown in Fig. 3a while that for the square grid is shown in Fig. 3b. As mentioned earlier, one can fail to detect numerical instabilities in the TLBE models if the number of lattice nodes J is too small; i.e., for J = 4 × 4 nodes one finds no instabilities with the spectral radius $\rho_\lambda = 1$. Saturated (asymptotic) values for ρ_λ, independent of the grid size, are found, provided the number of lattice nodes are

(I) hexagonal model, $\mathrm{J_{hex}} = 400 \times 400$;
(II) square mode, $\mathrm{J_{sq}} = 100 \times 100$.

The saturation of ρ_λ has been verified for several values of ε_0 on $\mathrm{J} = 840 \times 840$ (hexagonal) and 420×420 (square) grids. These results are shown as squares in Fig. 3.

We now examine the minimum kinematic viscosities that can be tolerated in order to avoid exciting these grid mode instabilities. Figure 4 shows $\rho_\lambda(\varepsilon_0)$ for several values of

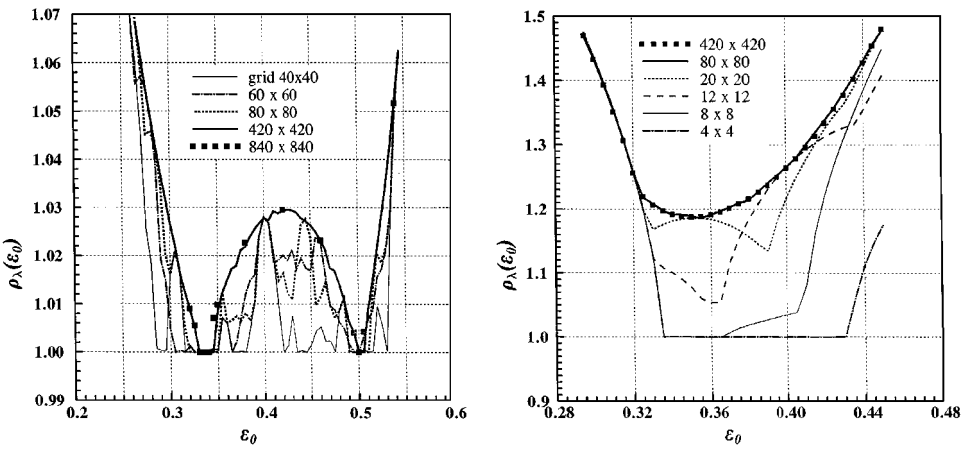

FIG. 3. The effects of lattice size on the spectral radius $\rho_\lambda(\varepsilon_0)$ for (a) hexagonal and (b) square grid. The spectral radius $\rho_\lambda(\varepsilon_0)$ becomes independent of the lattice size, provided (a) the hexagonal grid size $\geq 400 \times 400$ and (b) the square grid size $\geq 100 \times 100$.

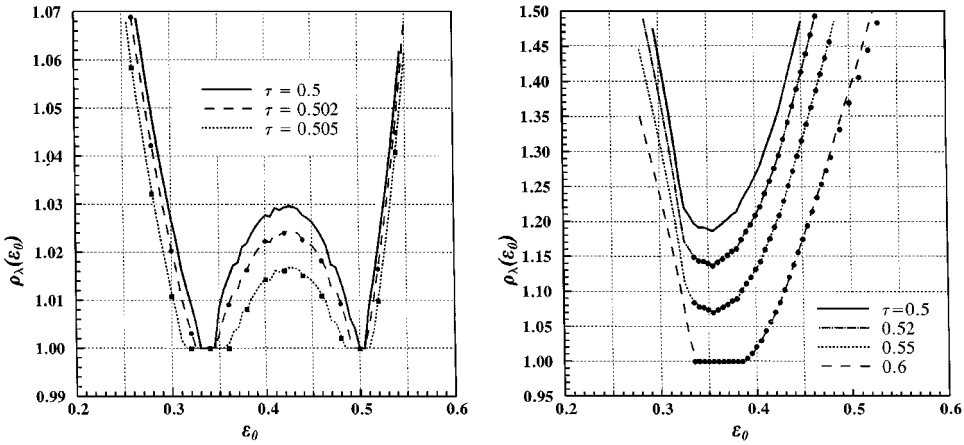

FIG. 4. The dependence of the spectral radius $\rho_\lambda(\varepsilon_0)$ on the collisional relaxation rate τ for the hexagonal and square lattice models. (a) For the hexagonal lattice, the dashed and dotted lines are derived from Eq. (35) and the full line for $\rho_\lambda(\tau = 0.5)$. The squares and dots indicate the values found directly by the method of powers for the respective values of τ and a 420×420 grid. (b) For the square (80×80) grid, the spectral radii solid curves are obtained directly by the method of powers, while the dotted lines are determined from Eq. (35), where applicable.

the relaxation parameter τ. We find substantial stable regions (i.e., $\rho_\lambda \leq 1$) in the energy density ε for

$$\text{(I) hexagonal grid: } \tau \approx 0.505, \quad \text{(II) square grid: } \tau \approx 0.6, \tag{33}$$

clearly showing that grid modes are easier to suppress if one is using the hexagonal lattice.

The spectral radius is obviously related to the specific choice of the equilibrium distribution functions (and possibly their departure from Maxwellians), but the discussion of such correlations is out of the scope of this paper. Here, we just note that when any $N_{pi}^{eq} < 0$ then the TLBE simulation is linearly unstable for any finite τ. This is the case for

$$\text{(I) hexagonal grid: } \varepsilon_0 \leq 0.25, \quad \text{(II) square grid: } \varepsilon_0 \leq 0.32 \tag{34}$$

as can be seen in the spectral radius $\rho_\lambda(\tau)$ for $\varepsilon_0 = 0.32$, Fig. 5. Within the least unstable region, the dependence of ρ_λ on τ can be well approximated by

$$\rho_\lambda(\tau) = \max\left\{1, \rho_\lambda\left(\frac{1}{2}\right) \cdot \left[1 - g(\varepsilon_0) \cdot \left(1 - \frac{1}{2\tau}\right)\right]\right\}. \tag{35}$$

For any ε_0, the coefficient $g(\varepsilon_0)$ can be calculated when ρ_λ is determined for two different values of τ.

In Fig. 4a, the spectral radii curves for relaxation parameter $\tau = 0.502$ and $\tau = 0.505$ were calculated using (35) with $g(\varepsilon_0) = 2(1.05 - \varepsilon_0)$, while the dots and squares were determined directly using the method of powers, (26). In Fig. 4b, all the spectral radii curves were determined by the method of powers, (26). The dots represent those values calculated from (35) with $g(\varepsilon_0) = 1.9\ \varepsilon_0 + 0.4$ for $\varepsilon_0 > 0.333$. The approximation (35) breaks down for $\varepsilon_0 > 0.5$ (see also Fig. 5).

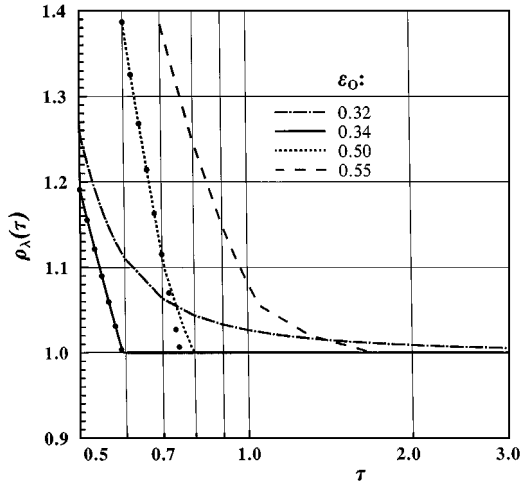

FIG. 5. The dependence of the spectral radius $\rho_\lambda(\tau)$ on the relaxation parameter τ for selected values of ε_0 for the square lattice. The dots are obtained from Eq. (35).

From (35) we can determine $\tau_{\min}$, the minimum relaxation parameter τ for which the spectral radius $\rho_\lambda = 1$ and hence, from (32) the maximum Reynolds number achievable in these TLBE models for a particular grid size $n_\alpha = N$ and macroscopic velocity u. These maximal Reynolds numbers for the hexagonal (R_H) and square (R_R) are shown in Fig. 6 for $u = 0.1$. In the range where (35) is invalid, R_R was determined from $\tau_{\min}$ obtained directly using the method of powers. It is clear that the hexagonal lattice provides much better numerical stability at high Reynolds numbers than the square lattice for the two TLBE models examined here.

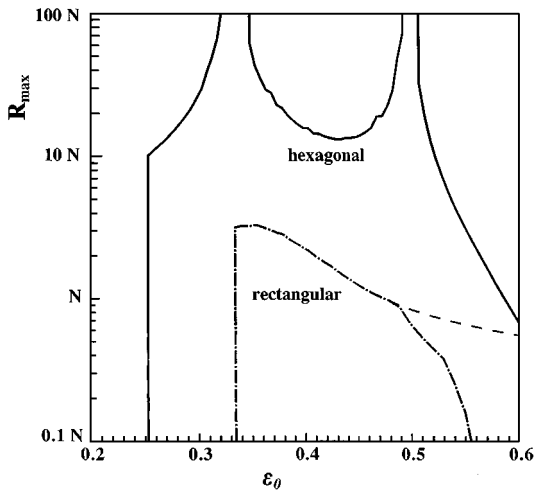

FIG. 6. The maximum achievable Reynolds number for the 13-bit 2D hexagonal (full line) and square (dash-dot) TLBE lattice models [11, 13]. The lattice size $n_\alpha = N$. The dashed line indicates the region where Eq. (35) starts to fail for the square (i.e., rectangular) grid. The hexagonal lattice provides much better numerical stability at high Reynolds numbers than the square lattice.

It is possible that the maximal Reynolds number achievable due to the onset of grid instabilities may be somewhat lower due to nonlinear effects. In particular, the energy density ε is not a constant in the full TLBE simulation and its variations must be kept within the stability limits. The allowed stability window for ε will be reduced as one increases the value of the macroscopic velocity u. However, lowering u lowers the Reynolds number, (32).

From our analysis of other TLBE models, it seems that the numerical stability gets worse as the number of speeds in the model are increased. This was seen in the stability patterns of a 2-speed 17-bit octagonal lattice compared to the 3-speed 13-bit square lattice. These results will be published elsewhere.

For the quasi-incompressible LBE models, which achieve closure at the momentum level, one can formally apply the same linearization procedure as outlined in Section 2. The coefficients A and B in Eq. (5) now become constants and the term containing the derivative A_p' vanishes; ε, in the definition of the coefficients A and B, can be retained as a free numerical parameter (with no physical meaning since there is no energy equation in LBE models). With these coefficient restrictions, we have considered a 13-bit square LBE model similar to that discussed earlier and found that this LBE model is linearly stable (spectral radius $\rho_\lambda = 1$) for $\tau = 0.5$ throughout the entire region in which the equilibrium distribution functions are positive (i.e., in the range $0.33 < \varepsilon < 0.67$). This is consistent with the result [19] that, under the assumption of positive equilibrium distribution, an H-theorem can be proved for quasi-incompressible LBE.

5. CONCLUSIONS

We have considered the linear stability of TLBE using the method of powers and applied our analysis to two 2-speed 13-bit TLBE models [11, 13]. With respect to the maximal achievable Reynolds number, the numerical stability of TLBE model based on the square lattice [13] was an order of magnitude worse than that for the hexagonal lattice [11].

For strong turbulence modeling, the current TLBE modeling [11–13] may have to be revised. One promising alternative has been suggested by He *et al.* [20] in which the spatial and (microscopic) velocity grids are decoupled. This allows not only for nonuniform spatial grid but a technique to increase the Reynolds number through interpolation techniques. Some care must be taken to ensure that the interpolation techniques that reconnect the spatial and velocity grids does not introduce additional viscosity and, hence, a reduced Reynolds number. Additional viscosity and reduced Reynolds number has been seen when we attempted to suppress the grid instabilities by either smoothing the distributions or upgrading the time derivative in TLBE to second-order accuracy.

These TLBE models [11, 13] which utilize the single relaxation time scalar BGK collision operator, have an invariant value for the Prandtl number ($\mathrm{Pr} = \mu/\kappa$). To simulate flows with a variable Prandtl number, one can generalize to a matrix collision operator whose eigenvalue properties allow a trivial matrix inversion as for the BGK scalar operator [21]. We have performed TLBE simulations and seen the effects of a variable Prandtl number on the evolution of density, temperature, and vorticity contours, as well as numerical stability analysis. This will be reported elsewhere [22].

ACKNOWLEDGMENTS

This work was supported by the U.S.–Czechoslovak Science and Technology Program Grant 930 66, as well as by the DoE.

REFERENCES

1. U. Frisch, B. Hasslacher, and Y. Pomeau, *Phys. Rev. Lett.* **56**, 1505 (1986).
2. U. Frisch, D. d'Humieres, B. Hasslacher, P. Lallemand, Y. Pomeau, and J.-P. Rivet, *Complex Syst.* **1**, 649 (1987).
3. S. Wolfram, *J. Stat. Phys.* **45**, 19 (1986).
4. H. Chen and W. Matthaeus, *Phys. Fluids* **30**, 1235 (1987).
5. J. M. V. A. Koelman, *Europhys. Letts.* **15**, 603 (1991). [S. Chen, H. Chen, D. Martinex, and W. Matthaeus, *Phys. Rev. Lett.* **67**, 3776 (1991); Y. H. Qian, D. d'Humieres, and P. Lallemand, *Europhys. Lett.* **17**, 479 (1992)]
6. M. Henon, *Complex Syst.* **1**, Appendix (1987). [H. Chen, *J. Stat. Phys.* **81**, 347 (1995)]
7. M. G. Ancona, *J. Comput. Phys.* **115**, 107 (1994).
8. S. Hou, Q. Zou, S. Chen, G. Doolen, and A. C. Cogley, *J. Comput. Phys.* **118**, 329 (1995). [L. Luo, unpublished]
9. Y. H. Qian and S. A. Orszag, *Europhys. Lett.* **21**, 255 (1993).
10. Y. Chen, Ph.D. thesis, University of Tokyo, 1994.
11. F. J. Alexander, S. Chen, and J. D. Sterling, *Phys. Rev. E* **47**, R2249 (1993).
12. Y. Chen, H. Ohashi, and M. Akiyama, *Phys. Rev. E* **50**, 2776 (1994).
13. Y. H. Qian, *J. Sci. Comput.* **8**, 231 (1993).
14. G. Vahala, P. Pavlo, L. Vahala, and H. Chen, *Phys. Lett. A* **202**, 376 (1995).
15. G. Vahala, P. Pavlo, L. Vahala, and M. Soe, *Czech J. Phys.* **46**, 1063 (1996).
16. R. Benzi, S. Succi, and M. Vergassola, *Phys. Repo.* **222**, 145 (1992).
17. J. D. Stirling and S. Chen, *J. Comput. Phys.* **123**, 196 (1996).
18. A. Raalston, *A First Course in Numerical Analysis* (McGraw–Hill, New York, 1965). [Czech edition, Academia, Prague, 1978]
19. Y. H. Qian, Ph.D. thesis, Universitè de Paris, 1990.
20. X. He, L. Luo, and M. Dembo, *J. Comput. Phys.* **129**, 357 (1996).
21. H. Chen, C. Teixeira, and K. Molvig, *Int. J. Modern Phys. C* **8**, 675 (1997).
22. M. Soe, G. Vahala, P. Pavlo, H. Chen, and L. Vahala, unpublished.